

Nonlinear dynamics in non-volatile locally-active memristor for periodic and chaotic oscillations

Wen-Yu Gu(谷文玉), Guang-Yi Wang(王光义), Yu-Jiao Dong(董玉姣), Jia-Jie Ying(应佳捷)

Citation: Chin. Phys. B . 2020, 29(11): 110503 . **doi:** 10.1088/1674-1056/ab9ded
Journal homepage: http://cpb.iphy.ac.cn; http://iopscience.iop.org/cpb

What follows is a list of articles you may be interested in

Energy feedback and synchronous dynamics of Hindmarsh-Rose neuron model with memristor

K Usha, P A Subha

Chin. Phys. B . 2019, 28(2): 020502 . **doi:** 10.1088/1674-1056/28/2/020502

A generalized model of TiO_x-based memristive devices andits application for image processing

Jiangwei Zhang(张江伟), Zhensen Tang(汤振森), Nuo Xu(许诺), Yao Wang(王耀), Honghui Sun(孙红辉), Zhiyuan Wang(王之元), Liang Fang(方粮)

Chin. Phys. B . 2017, 26(9): 090502 . **doi:** 10.1088/1674-1056/26/9/090502

Attempt to generalize fractional-order electric elements to complex-order ones

Gangquan Si(司刚全), Lijie Diao(刁利杰), Jianwei Zhu(朱建伟), Yuhang Lei(雷妤航), Yanbin Zhang(张彦斌)

Chin. Phys. B . 2017, 26(6): 060503 . **doi:** 10.1088/1674-1056/26/6/060503

Dynamical characteristics of an HP memristor based on an equivalent circuit model in a chaotic oscillator

Yuan Fang, Wang Guang-Yi, Wang Xiao-Yuan

Chin. Phys. B . 2015, 24(6): 060506 . **doi:** 10.1088/1674-1056/24/6/060506

Mapping equivalent approach to analysis and realization of memristor-based dynamical circuit

Bao Bo-Cheng, Hu Feng-Wei, Liu Zhong, Xu Jian-Ping

Chin. Phys. B . 2014, 23(7): 070503 . **doi:** 10.1088/1674-1056/23/7/070503

Nonlinear dynamics in non-volatile locally-active memristor for periodic and chaotic oscillations*

Wen-Yu Gu(谷文玉), Guang-Yi Wang(王光义)†, Yu-Jiao Dong(董玉姣), and Jia-Jie Ying(应佳捷)

Institute of Modern Circuits and Intelligent Information, Hangzhou Dianzi University, Hangzhou 310018, *China*

(Received 22 April 2020; revised manuscript received 7 June 2020; accepted manuscript online 18 June 2020)

Complexity and abundant dynamics may arise in locally-active systems only, in which locally-active elements are essential to amplify infinitesimal fluctuation signals and maintain oscillating. It has been recently found that some memristors may act as locally-active elements under suitable biasing. A number of important engineering applications would benefit from locally-active memristors. The aim of this paper is to show that locally-active memristor-based circuits can generate periodic and chaotic oscillations. To this end, we propose a non-volatile locally-active memristor, which has two asymptotically stable equilibrium points (or two non-volatile memristances) and globally-passive but locally-active characteristic. At an operating point in the locally-active region, a small-signal equivalent circuit is derived for describing the characteristics of the memristor near the operating point. By using the small-signal equivalent circuit, we show that the memristor possesses an edge of chaos in a voltage range, and that the memristor, when connected in series with an inductor, can oscillate about a locally-active operating point in the edge of chaos. And the oscillating frequency and the external inductance are determined by the small-signal admittance $Y(\mathrm{i}\omega)$. Furthermore, if the parasitic capacitor in parallel with the memristor is considered in the periodic oscillating circuit, the circuit generates chaotic oscillations.

Keywords: memristor, chaos local activity, Hopf bifurcation

PACS: 05.45.–a, 05.45.Jn, 05.45.Pq **DOI:** 10.1088/1674-1056/ab9ded

1. Introduction

There are three kinds of basic circuit elements in traditional circuits: resistor, capacitor, and inductor, which can be defined by the mathematical relations connecting the four basic circuit variables: current, voltage, charge, and magnetic flux. In 1971, Chua proposed the fourth basic circuit element, *i.e.*, memristor described by the relation between charge q and magnetic flux φ from the perspective of completeness of circuit theory.[1] In 1976, Chua further extended the notion of memristor to memristive systems.[2] However, due to the lack of practical memristor implementation it has not received much attention for nearly 30 years since it was first proposed. It was not until the HP Labs announced the preparation of a two-terminal device with memristor characteristics and reported its research in *Nature* in 2008, that the memristor received immense worldwide attention from both academia and industry.[3] This has led to a series of researches on how to use the characteristics of memristors to design nonlinear circuits,[4,5] intelligent computers,[6,7] and neural networks.[8]

A memristor is a nonlinear resistor with memory, according to which we can design chaotic circuits, which can be used in the chaotic neural networks and various information encryption systems.[9–11] In Ref. [4] proposed was a memristor-based multi-scroll hyperchaotic system, which has complex dynamic behaviors such as coexisting attractors, hidden coexisting attractors and multistability. In Ref. [12], a memristor based circuit was introduced, which exhibits multistability, transient dynamics and anti-monotonicity. Furthermore, by using the excellent characteristics of the chaotic memristor system a chaotic image encryption algorithm based on dynamic DNA manipulation and dynamic diffusion (CIEA-4D) was designed, which can improve the security of the encryption algorithm and has a high computing rate. At present, there are few studies on the generation mechanism of chaotic oscillation. Fortunately, Chua proposed that local-activity was the origin of all complexities,[13] and locally-active memristor-based chaotic circuits can better reveal the mechanism of generating the complex chaotic phenomena.

Locally-active memristive system can produce more complex and richer dynamics, which is of great significance for amplifying small signals and then maintaining the oscillation in nonlinear dynamic systems.[13,14] Based on the concept of local activity, Chua found a minuscule region called the edge of chaos, in which complex phenomena such as creativity, intelligence, and chaos, may emerge.[13,15]

A simplest chaotic circuit in which used are only an active memristor, a capacitor and an inductor in series, was designed by Muthuswamy and Chua.[16] Thereafter, Chua introduced the notion of locally-active memristor, which is defined for any memristor that has a negative memristance at some values of voltage across the memristor.[17] In Ref. [17], Chua proposed a passive but locally-active memristor, which can oscillate periodically about a locally-active operating point, when it is connected in series with a linear inductor and a battery.[15,18]

*Project supported by the National Natural Science Foundation of China (Grant No. 61771176).

†Corresponding author. E-mail: wanggyi@163.com

© 2020 Chinese Physical Society and IOP Publishing Ltd

Furthermore, In Ref. [19] proposed was a locally-active memristor model, based on which a simple chaotic circuit that contains only an inductor, a capacitor and the memristor in parallel was designed. The chaotic phenomenon means the ability of the locally-active memristor to amplify infinitesimal signal and generate chaos.

If a non-volatile memristor has two stable memristance states, it can be used to present logic states to realize non-volatile memories and logic operation circuits. In Ref. [20], a locally-active memristor was proposed and its state switching mechanism realizing the fast switching between different memristance states was discussed in detail. Then in Refs. [21,22] the authors proposed a locally-active memristor with 5 equilibrium points and a locally-active memristor with 7 equilibrium points, respectively. However, in Ref. [21], only the locally-active memristor-based periodic oscillation was found, and in Ref. [22], only the switching strategy of the proposed model was studied. Hence neither involves the complex chaotic oscillation, which is the important problem in exploring the complex mechanism of locally-active memristor based systems.

Memristors also have great potential applications in neural networks. The human brain is very powerful and complex, consisting of countless neurons and synapses. In 2014, Sah *et al.* presented that the human brain is composed of memristors,[6] showing that memristors have similar characteristics to biological synapses. Furthermore, from the perspective of information processing, synapses and neurons are comprized of locally-passive memristors and locally-active memristors, respectively.[13]

Using Chua's local activity and edge of chaos theory, in Ref. [23] studied are the generation and control of complex behaviors in a cellular neural network based on NbO_x locally-active memristor under coupled conditions. To study the generation and control of this complex behavior is the premise of simulating the neural cell information processing, and provides a theoretical basis for memristors in simulating cellular synapses.

In Ref. [13] reported was a locally-active nanoscale NbO_2 Mott memristor, which has both current- and temperature-controlled negative differential resistances (NDRs). And an intrinsic coupled oscillator incorporated into such a memristor can generate chaotic oscillations. Furthermore, computational efficiency of a hardware-implemented Hopfield neural network can be improved by investigating the memristor-based intrinsic chaotic oscillators.[13]

There is evidence that neural networks, when operated at the edge of chaos, can exhibit enhanced computational efficiency.[13] So, a memristor-based chaotic oscillator that can be incorporated into a memristor-based neural-inspired circuit may be a good scheme for future computational systems. Fortunately, locally-active memristor is a perfectly suitable candidate for constructing both chaotic oscillators and neural networks. At present, however, there is a lack of research on locally-active memristor-based chaotic oscillators and neural networks.

In order to explore the edge of chaos regime and nonlinear dynamic characteristics of locally-active memristors, a new locally-active generic memristor model is proposed in this paper. This new memristor has local activity with two non-volatile memductances. Using small-signal circuit of the memristor, we design a periodic oscillator, whose dynamics including Hopf bifurcation and periodic oscillations are analyzed in detail. We also design a chaotic circuit based on the proposed memristor, which is used to uncover the mechanism of complexity. It is found that the proposed locally-active memristor that operates on the edge of chaos regime can generate a complex chaotic oscillation, which is the most important finding in this paper.

2. Locally-active memristor model

All memristors can be divided into four categories, namely ideal memristor, ideal generic memristor, generic memristor, and extended memristor. When a memristor is driven by a voltage source (or current source), it is a voltage-controlled (or current-controlled) memristor.[17]

According to Chua's unfolding theorem,[24] a generic voltage-controlled memristor can be given by

$$\begin{cases} i_M = W(x)v_M, \\ \dfrac{\mathrm{d}x}{\mathrm{d}t} = f(x, v_M) = \displaystyle\sum_{k=-n_1}^{n_2} a_k x^k + \sum_{k=-m_1}^{m_2} b_k v_M^k \\ \qquad\qquad + \displaystyle\sum_{k=-p_1}^{p_2}\sum_{l=-q_1}^{q_2} c_{kl} v_M^k x^l, \end{cases} \tag{1}$$

where $W(x) = \sum_{k=-r_1}^{r_2} d_k x^k$ is the memductance of the memristor; x is the internal state variable; a_k, b_k, and c_{kl} are unfolding parameters, which can determine different generic memristor models from Eq. (1).

According to Eq. (1) and the Chua corsage memristor,[17] to make the memristor have both local activity and non-volatility characteristics, we define a mathematical model of a voltage-controlled locally-active generic memristor as follows:

$$\begin{cases} i = G(x)v = (x^2 + m)v, \\ \dfrac{\mathrm{d}x}{\mathrm{d}t} = h(x, v) = -x|x+\alpha| + |x+\beta| + v. \end{cases} \tag{2}$$

For the memductance function $G(x)$, m is a control parameter of the locally-active region, which can control the locally-active region of the memristor. In the state equation, α and β are the parameters to control the number of equilibrium points. Here, let $\alpha = -10$ and $\beta = 10$, then the memristor will

have 3 equilibrium points, in which there are 2 asymptotically stable equilibrium points, thereby exhibiting the non-volatility.

Any memristor, when driven by a zero-mean periodic voltage (or current) source, must have frequency-dependent pinched hysteresis loops in the v–i plane and coincident zero-crossing characteristics.[25,26] The memristor, when driven by a sinusoidal source $v(t) = A\sin(2\pi ft)$ with a amplitude of $A = 10$ V and frequencies $f = 0.5$ Hz, 2.5 Hz, and 500 Hz, exhibits the frequency-dependent pinched hysteresis loops, as shown in Fig. 1(a), where $m = 0$ and initial value of $x(0) = 0.5$. Observe all pinched hysteresis loops that pass through the origin (0, 0). As the frequency increases, the lobe area of the pinched hysteresis loop gradually decreases and shrinks into a straight line at a frequency of $f = 500$ Hz. When the voltage passes through the t axis, the current must also pass through the t axis at the red points in Fig. 1(b), showing the coincident zero-crossing signature. However, when the voltage waveform does not pass through the t axis, the current waveform can also pass through the t axis, which is described by the magenta points in Fig. 1(b), showing non-coincident zero-crossing signatures, which is one of the characteristics of a locally-active memristor.

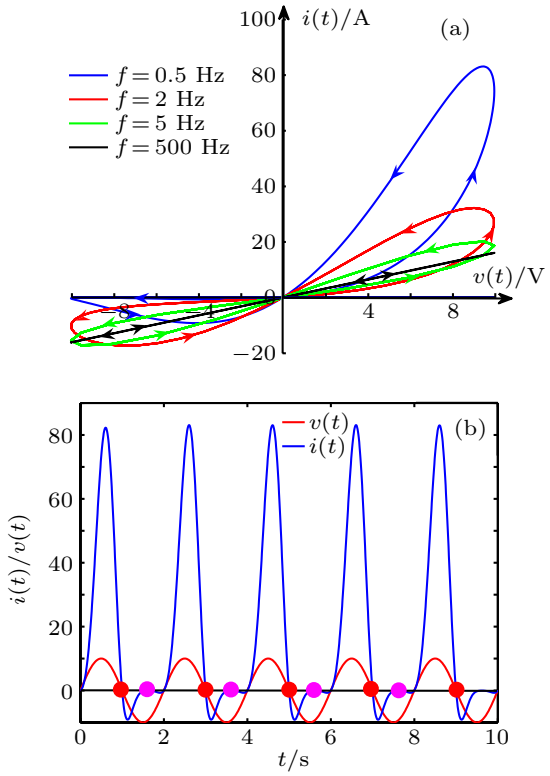


Fig. 1. (a) Pinched hysteresis loops driven by sinusoidal voltage with amplitude $A = 10$ V at $f = 0.5$ Hz, 2 Hz, 5 Hz, and 500 Hz, with $m = 0$ and initial state $x(0) = 0.5$; (b) time domain waveforms of input voltage (red) and output current (blue) at frequency $f = 2$ Hz.

3. Non-volatility and local activity of memristor

3.1. Non-volatility

According to Ref. [17], a memristor with a scalar state variable, if its power-off plot (POP) has two or more negative intersections with the x axis, it is a non-volatile memristor. The POP is a dynamic route map (DRM) on the $(\mathrm{d}x/\mathrm{d}t)$–$x$ plane when the voltage source is zero. The POP of the locally-active memristor determined by Eq. (2) can be solved by the following equation:

$$\frac{\mathrm{d}x}{\mathrm{d}t} = h(x,0) = -x|x-10| + |x+10|. \tag{3}$$

We plot the POP determined by Eq. (3) on the $(\mathrm{d}x/\mathrm{d}t)$–$x$ plane, as shown in Fig. 2.

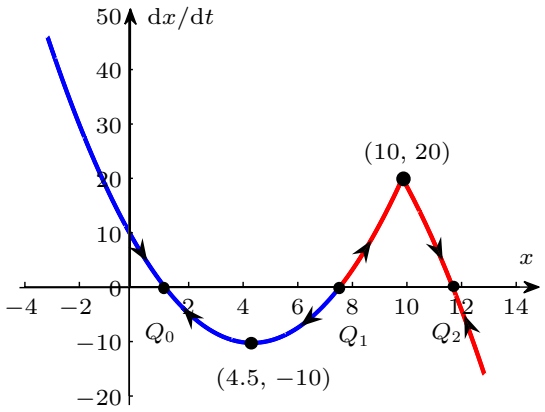


Fig. 2. POP of locally-active memristor.

Observe from Fig. 2 the POP that has 3 intersections with the x axis: Q_0 ($x = 1.298$), Q_1 ($x = 7.702$), and Q_2 ($x = 11.844$), where $\mathrm{d}x/\mathrm{d}t = 0$, and the arrowheads attached indicate the direction of motion of state variable x. Any initial state x on POP lying in the upper half plane, where $\mathrm{d}x/\mathrm{d}t > 0$, must move rightward along the POP. In contrast, any initial state x on POP located in the lower half plane must move leftward along the POP, because $\mathrm{d}x/\mathrm{d}t < 0$ there. It follows from the dynamical route on the POP in Fig. 2 that the equilibrium points Q_0 and Q_2 are asymptotically stable, while equilibrium point Q_1 is unstable.

Depending on the initial state $x(0)$, the memristor can exhibit two non-volatile states, namely,

$$x = \begin{cases} x(Q_0) = 1.298, & x(0) < 7.702, \\ x(Q_2) = 11.844, & x(0) > 7.702. \end{cases} \tag{4}$$

These two different stable states generate two corresponding stable memductances, that is,

$$W = \begin{cases} W(x(Q_0) = (7.702)^2 = 1.685S, & x(0) < 7.702, \\ W(x(Q_2) = (11.844)^2 = 140.280S, & x(0) > 7.702. \end{cases} \tag{5}$$

These two different stable memductances can be used to represent the binary states '0' and '1', one sate will remain unchanged until an appropriate external voltage is applied to the memristor to drive the stable equilibrium state to the other state. Therefore, this locally-active memristor can be used as a non-volatile binary memory.

3.2. Local activity

It is impossible to judge whether a generic memristor has locally-active property only through its hysteretic curve, because a generic memristor behaves like a nonlinear resistor in the regime of the direct current (DC) stable state,[26] and therefore we cannot measure the DC behavior by using the pinched hysteretic v–i curve under a periodic exciting signal. However, according to the DC V–I plot,[17] we can easily understand the inherent characteristics of the memristor and its local activity.

Let $\mathrm{d}x/\mathrm{d}t = 0$, $v = V$, and $x = X$, where V and X are the DC voltage input and corresponding state variable, respectively, in the state equation of Eq. (2), then we will obtain

$$V = \hat{v}(X) = X\,|X-10| - |X+10|\,. \tag{6}$$

Substituting Eq. (6) into the first equation of Eq. (2), we obtain

$$I = \hat{i}(X) = x^2\hat{v}(X) = X^3\,|X-10| - X^2\,|X+10|\,. \tag{7}$$

In the interval of $-2 \le X \le 12$, the DC V–I plot determined by Eqs. (6) and (7) is shown in Fig. 3.

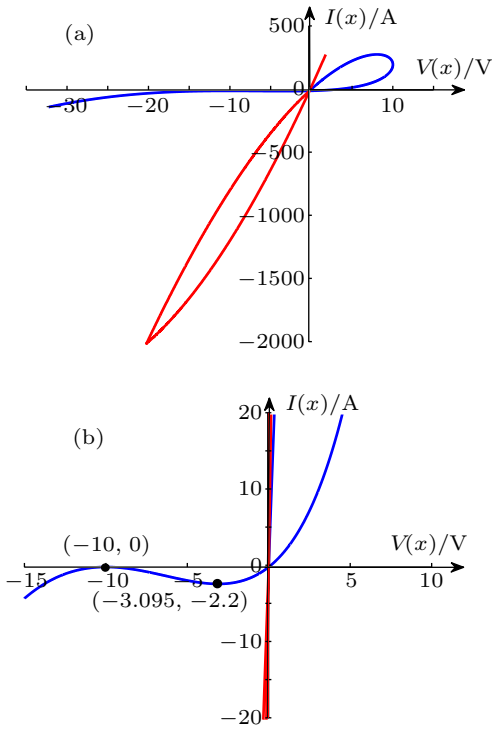


Fig. 3. (a) DC V–I plot of memristor (b) zoomed DC V–I plot near negative slope region.

This memristor (defined in Eq. (2)) is passive at DC V–I plot because all points on the plot lie in the 1st and 3rd quadrants where $VI \ge 0$.

From Fig. 3(a), we can observe that all points of the DC V–I plot lie in the 1st and 3rd quadrants where $V(x)I(x) \ge 0$, so this memristor is passive. However, it is locally-active in the interval of $-10\ \mathrm{V} < V < -3.095\ \mathrm{V}$, where the DC V–I plot has a negative slope (or negative differential conductance) over the interval as shown in Fig. 3(b).

4. Characteristics of locally-active region

The locally-active region is a non-linear region, where it is very complicated to implement rigorous analysis. To simplify the analysis, we can approximately linearize its equations near a DC operating point in the locally-active region. The linearization is derived by using the Taylor series about a DC operating point (V, I) of the memristor in its locally-active region. Then we use the small-signal equivalent circuit to analyze the local dynamic behavior of the memristor. For this purpose, we apply a small-signal input voltage δv to the DC operating point (V, I), which gives rise to the responses δx and δi,

$$\begin{aligned} v &= V + \delta v, \\ x &= X + \delta x, \\ i &= I + \delta i, \end{aligned} \tag{8}$$

where $X = x(Q)$, $V = v(Q)$, $I = i(Q)$, and X satisfies

$$\frac{\mathrm{d}x}{\mathrm{d}t} = -X\,|X-10| + |X+10| + V = h(X,V) = 0. \tag{9}$$

A small-signal equivalent circuit for the DC operating point can be obtained by Taylor expansion and Laplace transformation.[27]

Equation (2) can be expanded into a Taylor series at the operating point $Q(X, V)$, and the higher-order minor terms are ignored and the resulting equations are given below:

$$\begin{aligned} i &= I + \delta i = a_0 + a_{11}\delta x + a_{12}\delta v, \\ \frac{\mathrm{d}x}{\mathrm{d}t} &= \frac{\mathrm{d}(X+\delta x)}{\mathrm{d}t} = h(X,V) + b_{11}\delta x + b_{12}\delta v, \end{aligned} \tag{10}$$

where

$$a_{11} = v\frac{\partial G(x)}{\partial x}|_Q = 2XV, \quad a_{12} = G(x)\frac{\partial v}{\partial v}|_Q = X^2, \tag{11}$$

$$\begin{aligned} b_{11} &= \frac{\partial}{\partial x}h(x,v)\,|_Q = \mathrm{sign}(X+10) - |X-10| \\ &\quad -X\cdot\mathrm{sign}(x-10), \\ b_{12} &= \frac{\partial}{\partial v}h(x,v)\,|_Q = 1. \end{aligned} \tag{12}$$

Applying Laplace transformation to Eq. (10), and let $L[\delta i(t)] = \hat{i}(s)$, $L[\delta x(t)] = \hat{x}(s)$, $L[\delta v(t)] = \hat{v}(s)$, then we will have

$$\begin{aligned} \hat{i}(s) &= a_{11}\hat{x}(s) + a_{12}\hat{v}(s), \\ s\hat{x}(s) &= b_{11}\hat{x}(s) + b_{12}\hat{v}(s). \end{aligned} \tag{13}$$

Solving Eq. (13), we obtain

$$\hat{i}(s) = a_{11}\frac{b_{12}\hat{v}(s)}{s-b_{11}} + a_{12}\hat{v}(s). \tag{14}$$

The small-signal admittance $Y(s,Q)$ about the operating point $Q(X,V)$ is as follows:

$$Y(s,Q) = \frac{\hat{i}(s)}{\hat{v}(s)} = \frac{a_{11}b_{12}}{s-b_{11}} + a_{12}. \tag{15}$$

Equation (15) can be recasted into the following form:

$$Y(s,Q) = \frac{1}{s\dfrac{1}{a_{11}b_{12}} + \dfrac{-b_{11}}{a_{11}b_{12}}} + a_{12} = \frac{1}{sL_x + R_x} + \frac{1}{R_y}, \tag{16}$$

where $L_x = 1/a_{11}b_{12}$, $R_x = -b_{11}/a_{11}b_{12}$, $R_y = 1/a_{12}$, and the values of L_x, R_x, and R_y are determined by the DC operating point $Q(X,V)$. Therefore, the characteristics of the memristor near the operating point $Q(X,V)$ in the locally-active region can be imitated by the small-signal equivalent circuit as shown in Fig. 4.

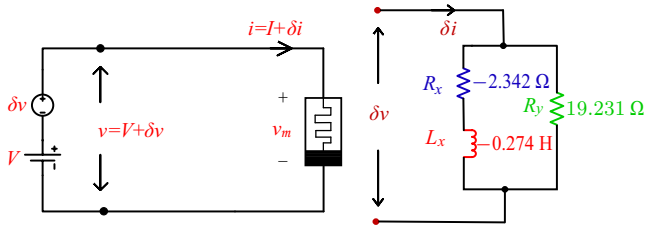


Fig. 4. Small-signal equivalent circuit of memristor at operating point $Q(X,V)$ under exciting voltage δv.

Let the static bias voltage across the memristor $V = -8$ V and $\mathrm{d}x/\mathrm{d}t = 0$, then from the state equation of Eq. (2) we will have

$$\frac{\mathrm{d}x}{\mathrm{d}t} = -X|X-10| + |X+10| - 8 = 0. \tag{17}$$

By solving Eq. (17), we obtain $X_Q = 0.228$, and then substituting it into Eqs. (11) and (12), we also obtain $a_{11} = -3.648$, $a_{12} = 0.052$, $b_{11} = -8.544$, $b_{12} = 1$. Substituting the values of a_{11}, a_{12}, b_{11}, and b_{12} into Eq. (16), we obtain the following parameters of the small-signal circuit:

$$L_x = \frac{1}{a_{11}b_{12}} = -0.274\ \mathrm{H},$$
$$R_x = \frac{-b_{11}}{a_{11}b_{12}} = -2.342\ \Omega,$$
$$R_y = \frac{1}{a_{12}} = 19.231\ \Omega. \tag{18}$$

5. Periodic oscillation of memristor

In order to observe the variation of small-signal admittance function $Y(s,Q)$ with DC bias voltage V, equation (15) can be rearranged as a function of bias voltage V as follows:

$$Y(s,V) = \frac{sa_{12} + [a_{11}b_{12} - a_{12}b_{11}]}{s - b_{11}} = \frac{K(s-z)}{(s-p)}, \tag{19}$$

where K is a constant, z and p are the zero and pole of $Y(s,V)$ at $V_Q = V$, respectively, specifically,

$$z = -\frac{a_{11}b_{12} - a_{12}b_{11}}{a_{12}}, \quad p = b_{11}, \quad K = a_{12}. \tag{20}$$

The pole and zero varying with operating point voltage V are shown in Fig. 5.

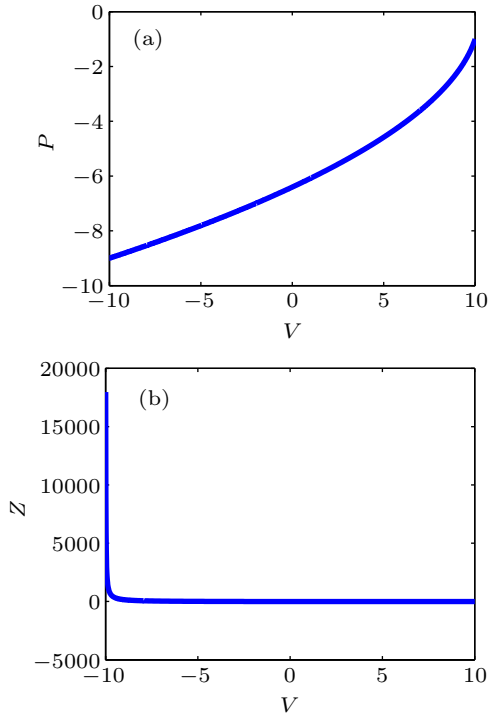


Fig. 5. The pole-zero diagram of the memristor in the voltage range of $-10 \le V \le 10$.

According to Hopf bifurcation theory,[15] to design an oscillator a pair of conjugate poles on the imaginary axis is needed. However, the admittance $Y(s,V)$ has only one real pole. Therefore, to make the circuit oscillate, it is necessary to add at least one capacitor or inductor to the memristor.

It can be observed from Fig. 4 that since the small-signal equivalent circuit of the memristor contains a negative inductance, only a positive linear inductance L has to be added in series with the memristor in order to make the composite circuit oscillate at a certain frequency. For determining the value of L, we need to determine the oscillating frequency of the composite circuit by calculating the frequency response $Y(\mathrm{i}\omega,V)$ of the memristor.

Substituting $s = \mathrm{i}\omega$ into Eq. (19), the admittance function $Y(\mathrm{i}\omega,V)$ is obtained as follows:

$$Y(\mathrm{i}\omega,V) = \frac{-b_{11}(a_{11}b_{12} - a_{12}b_{11}) + \omega^2 a_{12}}{b_{11}^2 + \omega^2} - \mathrm{i}\frac{\omega a_{11}b_{12}}{b_{11}^2 + \omega^2}. \tag{21}$$

The real and imaginary parts of admittance function $Y(\mathrm{i}\omega,V)$ at operating point $v = V$ are as follows:

$$\mathrm{Re}\,Y(\mathrm{i}\omega,V) = \frac{-b_{11}(a_{11}b_{12} - a_{12}b_{11}) + \omega^2 a_{12}}{b_{11}^2 + \omega^2}, \tag{22}$$

$$\mathrm{Im}\,Y(\mathrm{i}\omega,V) = -\frac{\omega a_{11}b_{12}}{b_{11}^2 + \omega^2}. \tag{23}$$

When the circuit oscillates, its energy consumption should be minimal, namely, $\mathrm{Re}\,Y(\mathrm{i}\omega^*,V)=0$, from which the oscillating frequency is determined by

$$\omega^*=\sqrt{\frac{b_{11}\,(a_{11}b_{12}-a_{12}b_{11})}{a_{12}}}. \tag{24}$$

When operating point bias voltage $V=-8$ V and the corresponding state variable $X=0.228$, from Eqs. (11) and (12) we obtain $a_{11}=-3.648$, $a_{12}=0.052$, $b_{11}=-8.544$, and $b_{12}=1$, then the oscillating frequency ω^* and the corresponding imaginary part $\mathrm{Im}\,Y(\mathrm{i}\omega^*,V)$ are calculated to be

$$\begin{aligned}&\omega^*(V,X)=\pm 22.9473877978,\\&\mathrm{Im}\,Y(\mathrm{i}\omega^*,V)=\pm 0.1396161112,\end{aligned} \tag{25}$$

which means that the memristor is capacitive at the operating point Q.

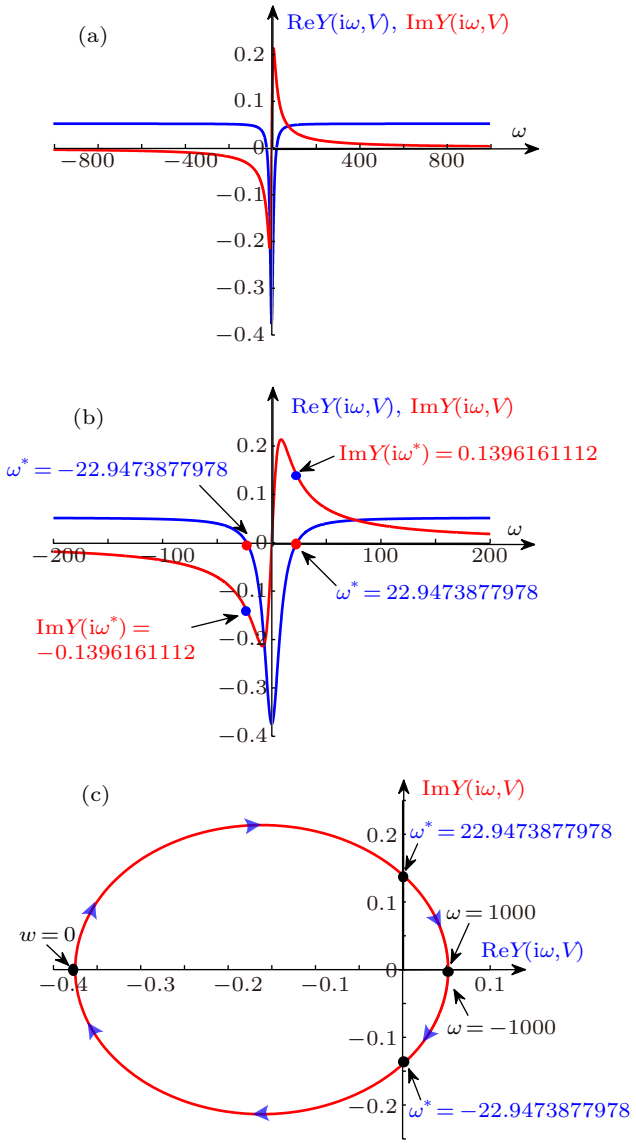


Fig. 6. Frequency response and Nyquist plot of the locally-active memristor at voltage $V=-8$ V, showing (a) real part $\mathrm{Re}\,Y(\mathrm{i}\omega,V)$ and imaginary $\mathrm{Im}\,Y(\mathrm{i}\omega,V)$ part of frequency response, (b) zoomed Fig. 6(a) in range -200 rad/s $\le\omega\le 200$ rad/s, and (c) Nyquist plot.

The real part $\mathrm{Re}\,Y(\mathrm{i}\omega,V)$ and the imaginary part $\mathrm{Im}\,Y(\mathrm{i}\omega,V)$ of the frequency response $Y(\mathrm{i}\omega,V)$ of the memristor determined by Eqs. (22) and (23) at voltage $V=-8$ V are shown in Fig. 6 in a range -1000 rad/s $\le\omega\le 1000$ rad/s.

It can follow from Fig. 6(b) that for the DC bias voltage $V=-8$ V, the real part $\mathrm{Re}\,Y(\mathrm{i}\omega^*,V)=0$ at $\omega^*=22.9473877978$ whereas the imaginary part $\mathrm{Im}\,Y(\mathrm{i}\omega^*,V)=0.1396161112$. The positive admittance of $\mathrm{Im}\,Y(\mathrm{i}\omega^*,V)$ indicates that the memristor is capacitive at the oscillating frequency ω^*, which requires a positive inductor L^* in series with the memristor to compensate for the imaginary part of admittance $Y(\mathrm{i}\omega^*,V)$ and make the total imaginary admittance of the composite circuit zero-valued. Therefore, the compensation inductance L^* should satisfy the following condition:

$$\frac{1}{\omega^*L^*}=\mathrm{Im}\,Y(\mathrm{i}\omega^*), \tag{26}$$

that is,

$$L^*=\frac{1}{\omega^*\,\mathrm{Im}\,Y(\mathrm{i}\omega^*)}=0.31212691\ \mathrm{H}. \tag{27}$$

The composite circuit composed of a locally-active memristor and a compensation inductor in series is shown in Fig. 7.

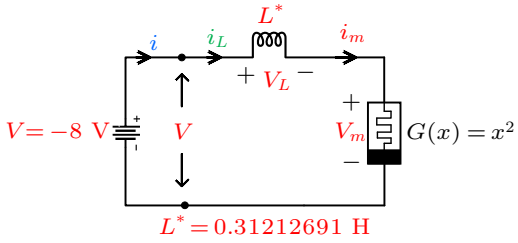


Fig. 7. Oscillating circuit composed of memristor operating in locally-active region.

6. Jacobian matrix $J(X,I_L;V)$ of locally-active memristor oscillator

To verify the oscillating circuit consisting of the locally-active memristor and the external inductor L^* as shown in Fig. 7, we can calculate the characteristic roots of the Jacobian matrix $J(X,I_L;V)$ of the oscillating circuit. It follows from Fig. 7 that $i=i_L=i_m$ and $v_L=v-v_m$, where $v_L=L^*\mathrm{d}i_L/\mathrm{d}t$ and $v_m=i_L/G(x)=i_L/x^2$. The state equations of the circuit are described by

$$\begin{aligned}\frac{\mathrm{d}x}{\mathrm{d}t}&=f(x,i_L)=-x|x-10|+|x+10|+\frac{i_L}{x^2},\\\frac{\mathrm{d}i_L}{\mathrm{d}t}&=g(x,i_L,v)=\frac{1}{L^*}\left(v-\frac{i_L}{x^2}\right).\end{aligned} \tag{28}$$

By solving $\mathrm{d}x/\mathrm{d}t=0$ and $\mathrm{d}i_L/\mathrm{d}t=0$, we can calculate the equilibrium point $Q(X,I_L;V)$ of Eq. (28), and the Jacobian matrix at $Q(X,I_L;V)$ is given by

$$J(X,I_L,V)=\left[\begin{array}{cc}\dfrac{\partial f(x,i_L)}{\partial x}&\dfrac{\partial f(x,i_L)}{\partial i_L}\\[2ex]\dfrac{\partial g(x,i_L,v)}{\partial x}&\dfrac{\partial g(x,i_L,v)}{\partial i_L}\end{array}\right]_Q$$

$$= \begin{bmatrix} \dfrac{\partial f(x,i_L)}{\partial x}\Big|_Q & \dfrac{1}{X^2} \\ \dfrac{2I_L}{L^*X^3} & -\dfrac{1}{L^*X^2} \end{bmatrix}, \tag{29}$$

where

$$\frac{\partial f(x,i_L)}{\partial x}|_Q = \operatorname{sign}(X+10) - |X-10| - X\operatorname{sign}(X-10) - \frac{2I_L}{X^3}. \tag{30}$$

Through Eq. (29), we can calculate the trajectories of the eigenvalues of Jacobian matrix $J(X,I_L;V)$ in a range $-20\ \text{V} \le V \le 20\ \text{V}$ as shown in Fig. 8, where $L^* = 0.31212691$ H, and the arrowheads in the trajectories indicate the motion directions of the two eigenvalues, λ_1 and λ_2, as the voltage V increases.

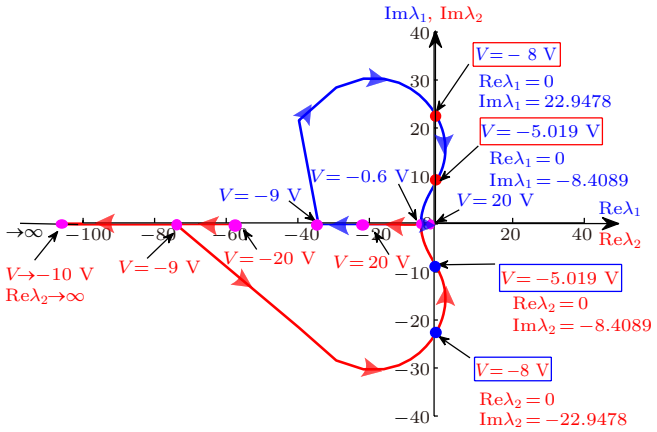


Fig. 8. Trajectories of eigenvalues in range of $-20\ \text{V} \le V \le 20\ \text{V}$.

From Fig. 8 we can see that the eigenvalue locus of Jacobian matrix $J(X,I_L;V)$ has a pair of complex conjugate eigenvalues $\lambda_1 = \pm 8.4089$ and $\lambda_2 = \pm 22.9478$ at $V = -5.019$ V and $V = -8$ V, respectively. The point at $V = -5.019$ V and $V = -8$ V on the imaginary axis are the Hopf bifurcation points where $\operatorname{Re}\lambda = 0$, and the region of $\operatorname{Re}\lambda > 0$ is the oscillating region.

7. Oscillating circuit admittance function $Y_c(s,V)$ and its pole-zero diagram

The total impedance of the oscillating circuit shown in Fig. 7 is the sum of the inductive reactance and the memductance. Considering formula (19), we obtain

$$Z_c(s,Q) = sL^* + 1/Y(s,Q) = \frac{s^2L^*a_{12} + s\left(L^*\left(a_{11}b_{12} - a_{12}b_{11}\right) + 1\right) - b_{11}}{sa_{12} + \left[a_{11}b_{12} - a_{12}b_{11}\right]}. \tag{31}$$

The total admittance of the oscillator circuit is given by

$$Y_c(s,Q) = \frac{1}{Z_c(s,Q)} = \frac{sa_{12} + \left(a_{11}b_{12} - a_{12}b_{11}\right)}{s^2L^*a_{12} + s\left(L^*\left(a_{11}b_{12} - a_{12}b_{11}\right) + 1\right) - b_{11}}, \tag{32}$$

which is rewritten as

$$Y_c(s,Q) = \frac{k(s-z_1)}{(s-p_1)(s-p_2)}, \tag{33}$$

where

$$z_1 = -\frac{a_{11}b_{12} - a_{12}b_{11}}{a_{12}}, \tag{34}$$

$$p_1 = \frac{-L^*\left[a_{11}b_{12} - a_{12}b_{11}\right] - 1 + \sqrt{\left(L^*\left[a_{11}b_{12} - a_{12}b_{11}\right] + 1\right)^2 + 4a_{12}L^*b_{11}}}{2a_{12}L^*}, \tag{35}$$

$$p_2 = \frac{-L^*\left[a_{11}b_{12} - a_{12}b_{11}\right] - 1 - \sqrt{\left(L^*\left[a_{11}b_{12} - a_{12}b_{11}\right] + 1\right)^2 + 4a_{12}L^*b_{11}}}{2a_{12}L^*}. \tag{36}$$

Substituting $s = \mathrm{i}\omega$ and Eqs. (11) and (12) into Eqs. (34)–(36), the real and imaginary part of the pole of $Y_c(s,V)$ are shown in Fig. 9, where $-20\text{V} \le V \le 20$ V, in which figures 9(a) and 9(b) show the trajectories of the real part of poles p_1 and p_2 as a function of voltage. Figure 9(c) shows a detailed view of the real part of poles p_1 and p_2, in the range of $-10\ \text{V} \le V \le 10\ \text{V}$; figure 9(d) dispalys the imaginary part of poles p_1 and p_2 as a function of voltage within the range of $-20\ \text{V} \le V \le 20\ \text{V}$; and figure 9(e) exhibits the trajectory of real and imaginary parts of the poles.

It is seen from Fig. 9 that real parts $\operatorname{Re} p_1$ and $\operatorname{Re} p_2$ of the admittance $Y_c(s,V)$ are almost less than zero for the voltage range of $-10\ \text{V} \le V \le 10\ \text{V}$ (Figs. 9(a)–9(c)) and only in the voltage range of $-8\ \text{V} < V < -5.3917$ V the real parts are greater than zero (Figs. 9(c) and 9(e)). We further find that the complex conjugate poles are located on the imaginary axis at voltages $V = -8$ V and $V = -5.3917$ V, where $\operatorname{Re} p_1 = 0$ and $\operatorname{Re} p_2 = 0$, meaning that $V = -8$ V and $V = -5.3917$ V are two Hopf bifurcation points,[18] and a periodic oscillation may occur via the Hopf bifurcation.

Figure 10 shows the loci of the real and imaginary parts of poles p_1 and p_2 as a function of the external inductance L. It is seen that $\operatorname{Re} p_1 = \operatorname{Re} p_2$ and $\operatorname{Im} p_1 = -\operatorname{Im} p_2$ for the range of $0.1511\ \text{H} \le L \le 0.6461$ H. At $L = L^* = 0.3121269$ H, $\operatorname{Re} p_1 = \operatorname{Re} p_2 = 0$, $\operatorname{Im} p_1 = 22.9485$, and $\operatorname{Im} p_2 = -22.9485$, which corresponds to a pair of complex conjugate poles that are the same as the pole at $V = -8$ V in Fig. 9(e).

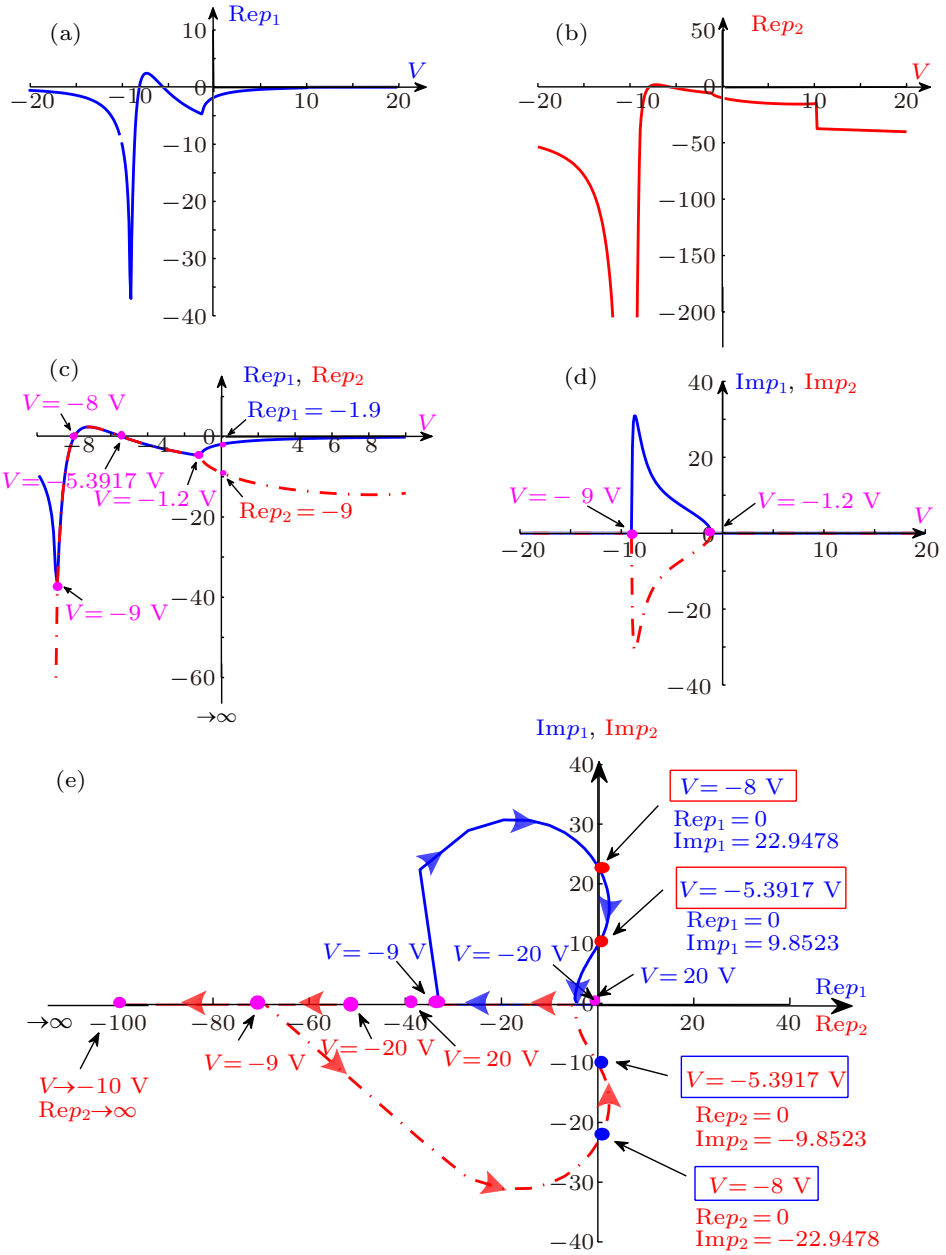


Fig. 9. Pole-zero diagrams of $Y_c(s,V)$ for (a) real part of pole p_1, (b) real part of pole p_2, (c) zoomed real part of poles p_1 and p_2 in the range of $-10\ \text{V} \le V \le 10\ \text{V}$, (d) imaginary part of poles p_1 and p_2, (e) the relationship between the real and imaginary parts of poles p_1 and p_2, in which the arrowheads indicate the movement direction of the pole as the voltage V increases.

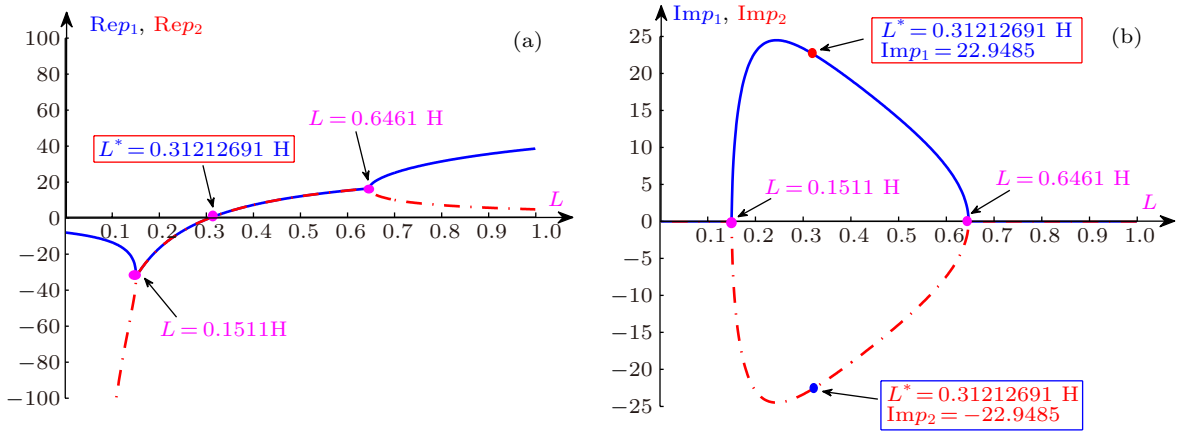


Fig. 10. Pole diagrams of admittance $Y_c(s,V)$ with external inductance L in a range of $0 < L < 1$ H, showing (a) real part of the poles, p_1 and p_2, and (b) imaginary part of the poles.

8. Edge of chaos and periodic oscillation

8.1. Edge of chaos

A nonlinear system on the edge of chaos has potential instability and therefore can generate complexity,[28–30] such as emergence, self-organization, chaos, *etc*. A nonlinear system is said to be on the edge of chaos if and only if all of its equilibrium points are locally active but asymptotically stable.[13] That is, the edge of chaos of this memristor can be determined by the two conditions as follows.[30]

(i) At the same equilibrium point $(X(V),I(V))$, the real part $\mathrm{Re}\,Y(\mathrm{i}\omega)$ of the frequency response of the admittance equation $Y(s,V)$ is less than zero ($\mathrm{Re}[Y(\mathrm{i}\omega)]<0$) for some $\omega\in(-\infty,\infty)$.

(ii) All poles of small-signal admittance of memristor $Y(s,V)$ at the equilibrium point $(X(V),I(V))$ are on the left-open plane where $\mathrm{Re}[s_p]<0$.

Obviously, conditions (i) and (ii) correspond to the locally activity and the asymptotical stability of the conditions of the edge of chaos, respectively. In order to verify the local activity of the memristor (condition (i)), the frequency responses of admittance $Y(\mathrm{i}\omega,V)$ of the memristor at different input voltages are shown in Fig. 11.

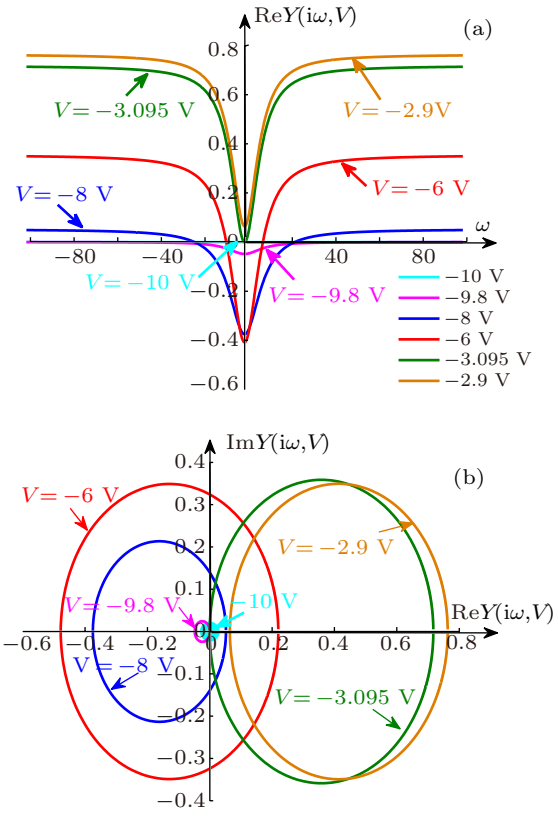


Fig. 11. Frequency response of admittance function $Y(\mathrm{i}\omega,V)$ with respect to ω, showing (a) real part curve of frequency response of memristor in a range of -100 rad/s $\le\omega\le$ 100 rad/s, and (b) Nyquist plot of memristor frequency response in a range of -1000 rad/s $\le\omega\le$ 1000 rad/s.

Figure 11(a) shows that when the input voltage $V=-10$ V, $\mathrm{Re}\,Y(\mathrm{i}\omega)=0$ for all values of ω and $\mathrm{Re}\,Y(\mathrm{i}\omega)<0$ for $V<-3.095$ V and some values of $\omega\in(-\infty,\infty)$. We also observe from Fig. 11(b) that when the input voltage $V=-10$ V, $\mathrm{Im}\,Y(\mathrm{i}\omega)=\mathrm{Re}\,Y(\mathrm{i}\omega)=0$, and $\mathrm{Re}\,Y(\mathrm{i}\omega)>0$ for $V>-3.095$ V, *i.e*., the locus of the frequency response $Y(\mathrm{i}\omega,V)$ is located on the right half plane for all values of ω.

It follows from Fig. 11 and the above analysis that the real part of the admittance function $Y(\mathrm{i}\omega,V)$ is less than zero, *i.e*., $\mathrm{Re}\,Y(\mathrm{i}\omega)<0$ in a range of $-10\mathrm{V}<V<-3.095$ V for some values of $\omega\in(-\infty,\infty)$, and therefore the memristor is locally active within the voltage range of $-10\mathrm{V}<V<-3.095\mathrm{V}$.[14]

To ensure that the memristor has an edge of chaos, the admittance $Y(s,V)$ of the memristor must satisfy condition (ii) as well. The poles of the admittance equation $Y(s,V)$ at the equilibrium point is shown in Fig. 5(a), from which we see that the poles are negative, *i.e*., $\mathrm{Re}(s_p)<0$ in the voltage range of -10 V $<V<-3.095$ V , implying that the poles of $Y(s,V)$ are in the left-half plane, and the admittance $Y(s,V)$ satisfies condition (ii).

According to the above analysis, we conclude that the admittance $Y(s,V)$ of the memristor satisfies both conditions (i) and (ii), and the memristor is on the edge of chaos in the voltage interval: -10 V $<V<-3.095$ V.

8.2. Periodic oscillation via Hopf bifurcation

Figure 8 presents the eigenvalues locus plot of the oscillating circuit shown in Fig. 7, from which we can see that the Jacobian matrix $J(X,I_L;V)$ of the circuit has a pair of complex conjugate eigenvalues on the imaginary axis at the DC operating point voltages $V=-8$ V and $V=-5.019$ V. As the DC voltage varies in the internal of -8 V $<V<5.095$ V, the eigenvalues can cross the imaginary axis and move to the right-half plane, and therefore the circuit loses its stability at $V=-8$ V and $V=-5.019$ V. Hence the DC operating point voltages $V=-8$ V and $V=-5.019$ V are two Hopf bifurcation points,[31] at which the circuit is no longer asymptotically stable.

The dynamics of the memristor-based oscillating circuit with respect to the DC operating points is shown in Fig. 12.

From Fig. 8 we see that when -8 V $<V<5.017$ V, the eigenvalue locus is located in the open right-half plane, where the real part of the eigenvalue, $\mathrm{Re}(\lambda)>0$, and the circuit oscillates or is in an unstable state.

It is observed from Fig. 12(a) that the circuit is in a stable state and converges to a stable equilibrium point $Q_0'(0.2163,-0.3790)$, as the voltage $V<-8$ V and equals -8.1 V that is near but to the left of the first Hopf bifurcation point $V=-8$ V. While the circuit generates a periodic oscillation to form a limit cycle as the DC voltage $V>-8$ V and equals -7.8 V that is near but to the right of the first Hopf bifurcation point, as shown in Fig. 12(b). Also it is observed from Figs. 12(c) and 12(d) that the circuit diverges from the initial state $(x(0),i_L(0))=(0.1,-0.1)$ and do not converge to any equilibrium point.

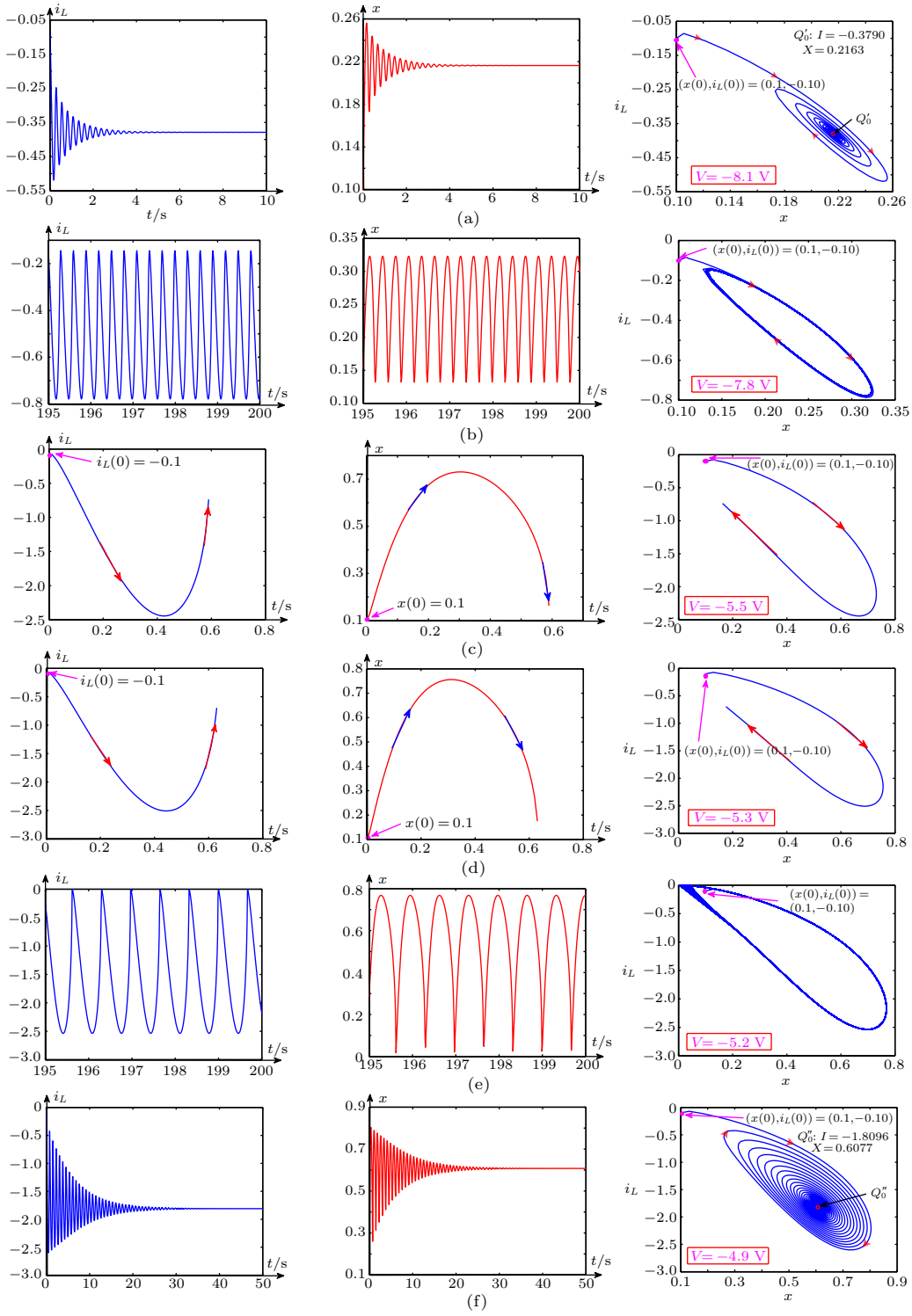


Fig. 12. Transient waveforms of state variable x and current i_L with different DC voltages, where initial states are $(x(0), i_L(0)) = (0.1, -0.1)$ (a) DC voltage $V = -8.1$ V, and transient waveforms converge to stable equilibrium point Q_0; (b) DC voltage $V = -7.8$ V, and the system oscillates to form a limit cycle; (c) DC voltage $V = -5.5$ V, and the system is in unstable state, diverging from initial state; (d) DC voltage $V = -5.3$ V, and the system is in unstable state, diverging from initial state; (e) DC voltage $V = -5.2$ V, and the system oscillates to form a limit cycle; (f) DC voltage $V = -4.9$ V, transient waveforms converge to stable equilibrium point Q_0'.

According to Figs. 12(e) and 12(f), the stability of the circuit changes near the second Hopf bifurcation point $V = -5.019$ V. Figure 12(e) shows that the circuit oscillates periodically again, as the voltage $V < -5.019$ V and equals -5.2 V, which is near but to the right of the second Hopf bifurcation point $V = -5.019$ V, while that the circuit converges to an another stable equilibrium point Q_0'' $(0.2163, -0.3790)$, as the voltage $V > -5.019$ V and equals -4.9 V, which is near but to the left of the second Hopf bifurcation point $V = -5.019$ V.

It follows that when the memristor operates at the edge of chaos of the memristor within the range of -10 V $< V <$ -3.095 V, it may generate periodic oscillation, indicating that

the memristor operating on the edge of chaos regime has potential instability and therefore generates oscillations.

9. From limit cycle to chaotic attractor

In the periodic oscillating circuit shown in Fig. 7, it operates in the locally-active region with the bias voltage of $V=-8$ V. If we design a chaotic oscillator on the basis of the periodic oscillator, so that it is convenient to make the memristor have a bias voltage of zero. To this end, we set the coefficient m in Eq. (2) to be -3, *i.e.*, the state-dependent Ohm's low becomes

$$\begin{aligned} &i=G(x)v=\left(x^2-3\right)v,\\ &\frac{\mathrm{d}x}{\mathrm{d}t}=h(x,v)=-x|x-10|+|x+10|+v. \end{aligned} \tag{37}$$

So the locally-active region will be expanded from the original $-10\ \mathrm{V}<V<-3.095\ \mathrm{V}$ to $-17.22\ \mathrm{V}<V<1.393\ \mathrm{V}$, which is analyzed as follows.

Let the second equation in Eq. (37) be zero for drawing the DC V–I plot, then we will obtain the relations V–X and the I–X as follows:

$$V=\breve{v}(X)=X|X-10|-|X+10|, \tag{38}$$

$$\begin{aligned} I&=\breve{i}(X)=(X^2-3)\breve{v}(X)\\ &=(X^2-3)(X|X-10|-|X+10|). \end{aligned} \tag{39}$$

In the interval of $-2\le X\le 4$, the relations V–X, I–X, and V–I are shown in Fig. 13.

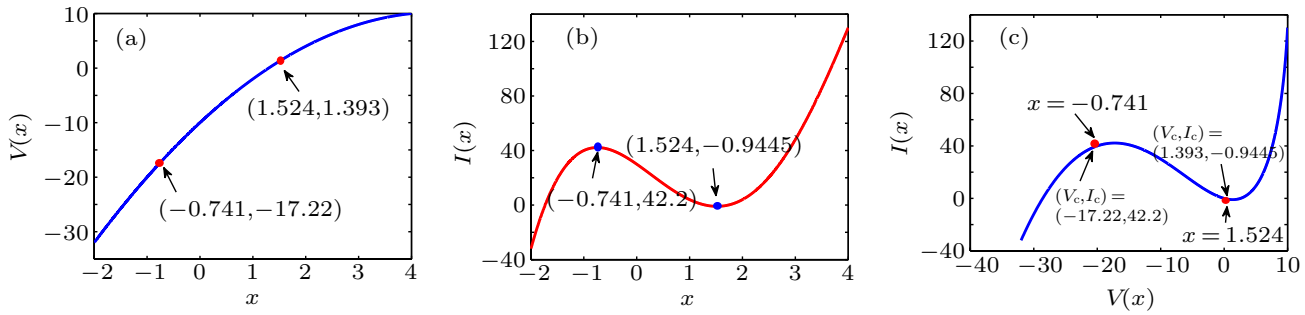


Fig. 13. Plots of the memristor determined by Eqs. (38) and (39): (a) $V=\breve{v}(X)$, (b) $I=\breve{i}(X)$, and (c) DC V–I plot.

By observing the DC V–I plot, we find that a negative slope appears in a range of $-0.741<x<1.524$, and the corresponding voltage V is in a range of $(-17.22,1.393)$, which is the locally-active region of the memristor that includes the locally-active operating point of $V=0$.

In the case that the memristor has a zero bias, if the parasitic capacitor connected with the memristor in parallel is considered, a chaotic oscillator can be obtained as shown in Fig. 14.

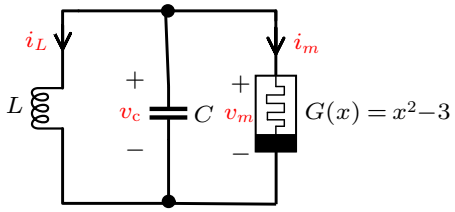


Fig. 14. Chaotic oscillator circuit based on locally-active memristor.

According to Eq. (37) and the Kirchhoff's law, the governing equation of the circuit is given by

$$\begin{cases} \dfrac{\mathrm{d}x}{\mathrm{d}t}=-x|x-10|+|x+10|+v_{\mathrm{C}},\\ \dfrac{\mathrm{d}v_{\mathrm{C}}}{\mathrm{d}t}=-\dfrac{1}{C}[(x^2-3)v_{\mathrm{C}}+i_L],\\ \dfrac{\mathrm{d}i_L}{\mathrm{d}t}=\dfrac{1}{L}v_{\mathrm{C}}. \end{cases} \tag{40}$$

Let $1/C=a$, $1/L=b$, $v_{\mathrm{C}}=y$, and $i_L=z$, equation (40) is rewritten as

$$\begin{cases} \dfrac{\mathrm{d}x}{\mathrm{d}t}=-x|x-10|+|x+10|+y,\\ \dfrac{\mathrm{d}y}{\mathrm{d}t}=-a[(x^2-3)y+z],\\ \dfrac{\mathrm{d}z}{\mathrm{d}t}=by. \end{cases} \tag{41}$$

Let $\mathrm{d}x/\mathrm{d}t=\mathrm{d}y/\mathrm{d}t=\mathrm{d}z/\mathrm{d}t=0$, then the equilibrium points of the system will be as follows:

$$s=\{(x,y,z)|x=X_Q,y=z=0\}, \tag{42}$$

where X_Q happens to be the equilibrium point of the memristor as shown in Fig. 2. It is observed from Fig. 2 and Eq. (42) that the circuit has three equilibrium points: $s_1=(1.2984,0,0)$, $s_2=(7.7015,0,0)$, and $s_3=(11.8443,0,0)$. Since the locally-active region of the memristor is $-0.741<x<1.524$, only equilibrium point $s_1=(1.2984,0,0)$ is in the locally-active region, where complex phenomena may occur in the neighborhood of the equilibrium point s_1. Linearizing Eq. (41) at the equilibrium point s_1, the Jacobian matrix can be obtained as follows:

$$J=\begin{pmatrix} -6.4032 & 1 & 0\\ 0 & 1.3142a & -a\\ 0 & b & 0 \end{pmatrix}. \tag{43}$$

And the corresponding characteristic equation is

$$\lambda^3 + (6.4032 - 1.3142a)\lambda^2 + (ab - 8.4151a)\lambda + 6.4032ab = 0. \quad (44)$$

Let $a = 2.13$ and $b = 11$, then the eigenvalues will be obtained to be $\lambda_1 = -6.4032$, $\lambda_2 = 1.3996 + 4.6337\mathrm{i}$, and $\lambda_3 = 1.3996 - 4.6337\mathrm{i}$, in which λ_2 and λ_3 are a pair of conjugate complex roots and their real parts are greater than zero, showing that equilibrium point s_1 is unstable, which satisfies one of the conditions for chaos. When $(x_0, y_0, z_0) = (1.298, 0.1, 0.1)$, $a = 2.13$ and $b = 11$, the circuit generates chaotic oscillations, and the corresponding Lyapunov exponents are $L_1 = 0.1630$, $L_2 = 0$, and $L_3 = -5.8877$. The chaotic attractor generated by the system is shown in Fig. 15, where figure 15(d) shows the pinched hysteresis curves of the memristor in the chaotic state, which are pinched at the origin but do not overlap each other. However, as the memristor voltage changes chaotically, these curves become a family and they never overlap, *i.e.*, they become a chaotic pinched hysteresis curve.

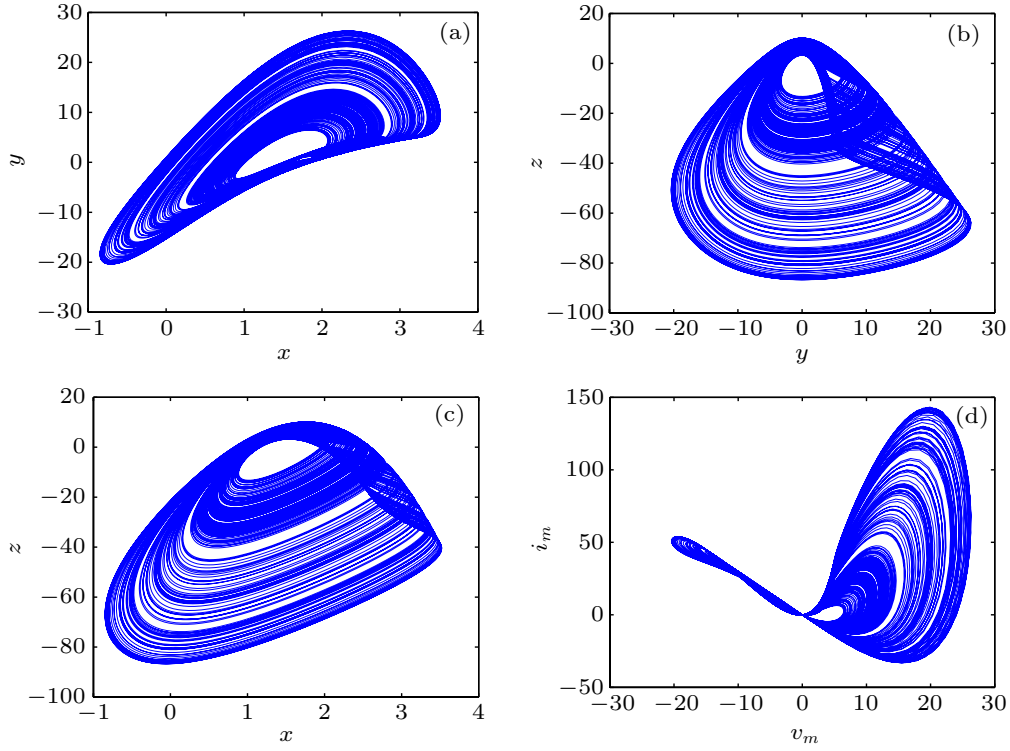


Fig. 15. Phase diagrams of this memristor-based chaotic oscillating circuit (a) x–y plane, (b) y–z plane, (c) x–z plane, and (d) chaotic pinched hysteresis loops of the memristor.

When the initial state $(x_0, y_0, z_0) = (1.298, 0.1, 0.1)$, the time domain waveform of the state variable x, the capacitor voltage v_C and the inductor current i_L of the memristor are shown in Fig. 16. Since the initial state $(x_0, y_0, z_0) = (1.298, 0.1, 0.1)$ is in the locally-active region of the locally-active memristor, the system can keep chaotic oscillating around the equilibrium point $s_1 = (1.2984, 0, 0)$, depending on the local activity of the memristor.

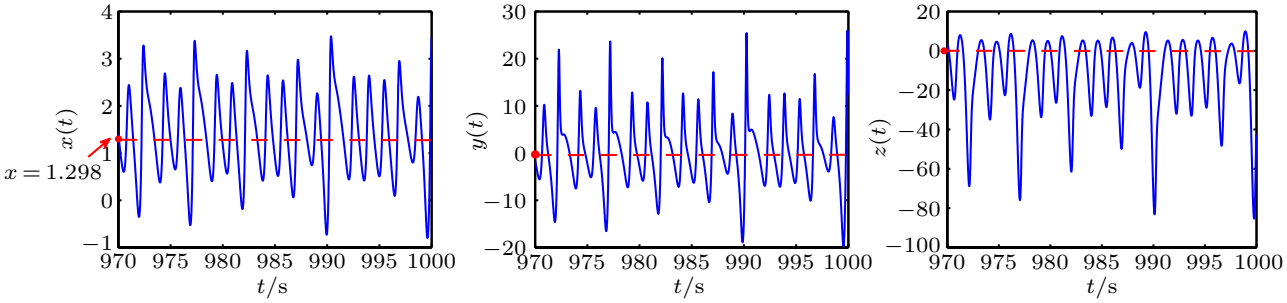


Fig. 16. Time domain waveform of memristor state variable x, capacitor voltage v_C, and inductor current i_L .

When circuit parameters $a = 2.13$ and $b = 11$, and the initial state $(x_0, y_0, z_0) = (4.5, 0.1, 0.1)$, the circuit oscillates chaotically, and its time domain waveforms and the x–y–z phase diagram of the chaotic circuit are shown in Fig. 17(a). When the circuit parameters are fixed but the initial state changes to $(x_0, y_0, z_0) = (11, 0.1, 0.1)$, the dynamics of the circuit converges to a stable point as shown in Fig. 17(b).

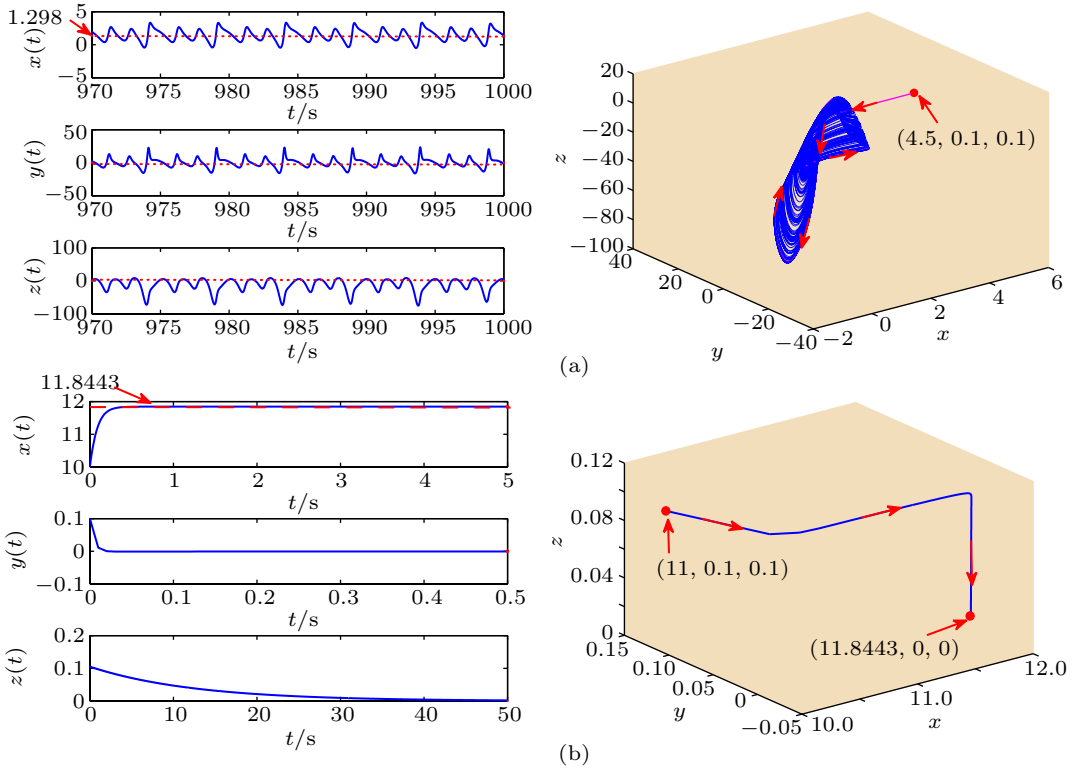


Fig. 17. (a) Time domain waveforms and x–y–z phase diagrams with circuit parameters fixed at (a) $(x_0, y_0, z_0) = (4.5, 0.1, 0.1)$; (b) $(x_0, y_0, z_0) = (11, 0.1, 0.1)$, but the initial values changed.

Table 1. Nonlinear dynamic characteristics of different initial conditions.

Initial condition	$(4.5, 0.1, 0.1)$	$(11, 0.1, 0.1)$
Equilibrium point	$(1.2984, 0, 0)$	$(11.8443, 0, 0)$
Memductance	negative	positive
Memristor characteristics	locally-active	locally-passive
Eigenvalues	$\lambda_1 = -6.4032$	$\lambda_1 = -292.342$
	$\lambda_2 = 1.3996 + 4.6337i$	$\lambda_2 = -12.689$
	$\lambda_3 = 1.3996 - 4.6337i$	$\lambda_3 = -0.080$
Lyapunov exponent	$(0.201 - 0.010 - 5.910)$	$(-0.113 - 12.630 - 31.280)$
System status	chaotic oscillation	asymptotically stability

It follows from Fig. 17 that the circuit can exhibit different dynamic behaviors, such as chaotic attractors and stable points, for a fixed set of circuit parameters and different initial values, which is called coexisting attractor. Thus there are coexisting attractors in the system, namely, this system has multi-stability.[12] Further analysis shows that for the initial condition $(x_0, y_0, z_0) = (4.5, 0.1, 0.1)$, the initially-excited chaotic orbit oscillates around the equilibrium point $X = 1.298$, which is exactly the asymptotically stable equilibrium point $X(Q_0) = 1.298$ (see Fig. 2) of the memristor, that is located in the locally-active region and on the edge of chaos of $-0.741 < X < 1.524$. So the circuit generates a complex chaotic motion, verifying that "locally-activity is the origin of complexity".[13]

The trajectories starting from the initial state $(x_0, y_0, z_0) = (11, 0.1, 0.1)$ eventually converges to a stable point (11.8443, 0, 0), which is exactly a stable point $X_2(Q_2)$ of the memristor (see Fig. 2). Because the initial value of the state variable $x(0) > 7.702$, we can see from Fig. 2 that the state x eventually goes to the asymptotically stable equilibrium point $X_2(Q_2)$ of the memristor as $t \to \infty$. Because the equilibrium point is located in the locally-passive region, it cannot generate chaotic oscillation.

The circuit dynamics with the two initial states, $(4.5, 0.1, 0.1)$ and $(11, 0.1, 0.1)$, including initial conditions, memristor equilibrium points, memristor characteristics, and circuit eigenvalues, Lyapunov exponents, are shown in Table 1.

With the circuit system parameters changing, the system is also in different states for a fixed set of initial values. Fixing initial condition $(x_0, y_0, z_0) = (1.298, 0.1, 0.1)$, when the circuit parameter a is changed within the range of [0.8, 2.2], the Lyapunov exponent spectrum and the bifurcation diagram with respect to a are shown in Fig. 18 (for the clarity, the third Lya-

punov exponential curve is not drawn here because its value is a smaller negative number).

From Fig. 18, we can observe that the system gradually turns from a periodic orbit to a chaotic state through a period-doubling bifurcation. In the region of $a \in [0.8, 2.2]$, the system switches between periodic orbit and chaotic orbit multiple times. When $a \in [0.8, 1.79]$, the system exhibits a periodic orbit; when $a \in (1.79, 1.86]$, it enters into chaos state through period doubling bifurcation; when $a \in (1.86, 1.87]$, it goes into a periodic window. The system performs multiple state transitions between chaotic and periodic states in the region $a \in [1.88, 2.2]$, and the corresponding chaotic and periodic orbits are shown in Fig. 19.

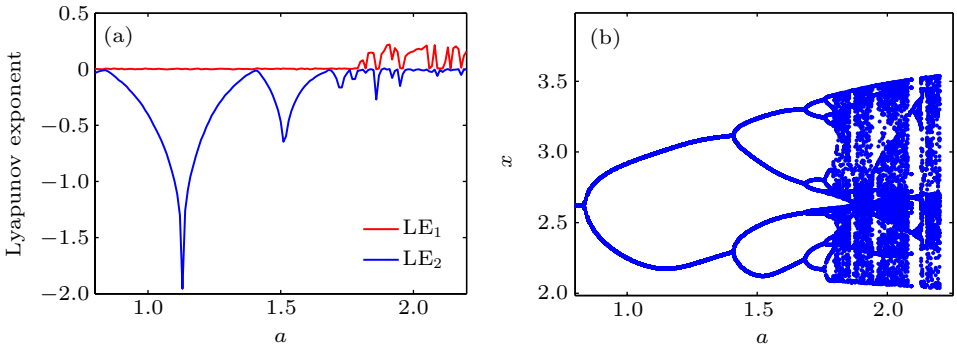


Fig. 18. (a) Lyapunov exponent (LE) spectrum and (b) bifurcation diagram varying with parameter a.

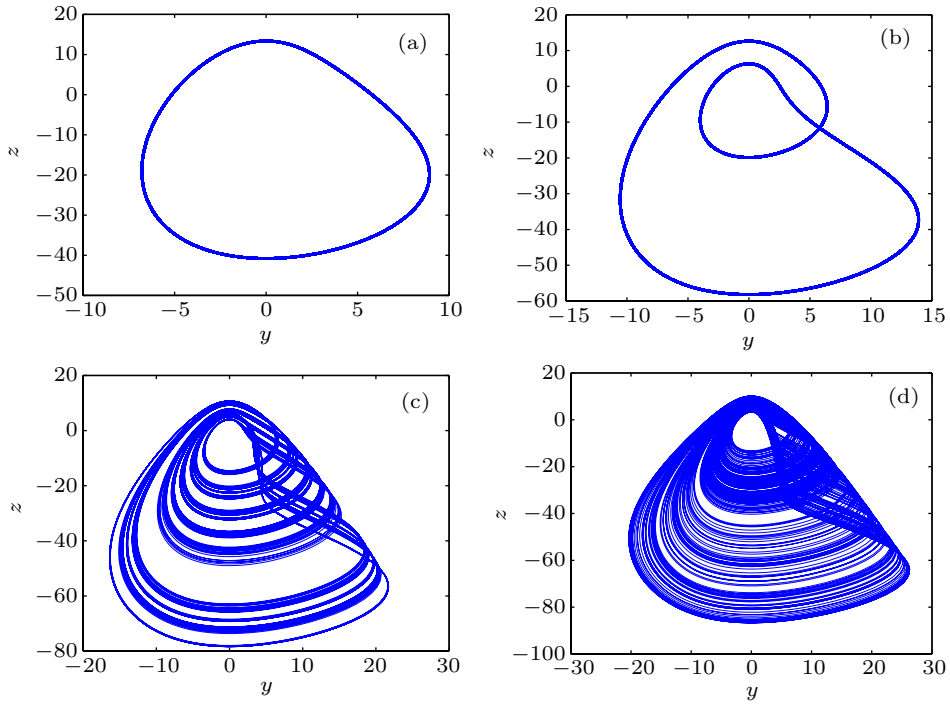


Fig. 19. Phase diagram changing with parameter a on the x–y plane: (a) $a = 0.8$, (b) $a = 1.2$, (c) $a = 1.793$, and (d) $a = 2.13$.

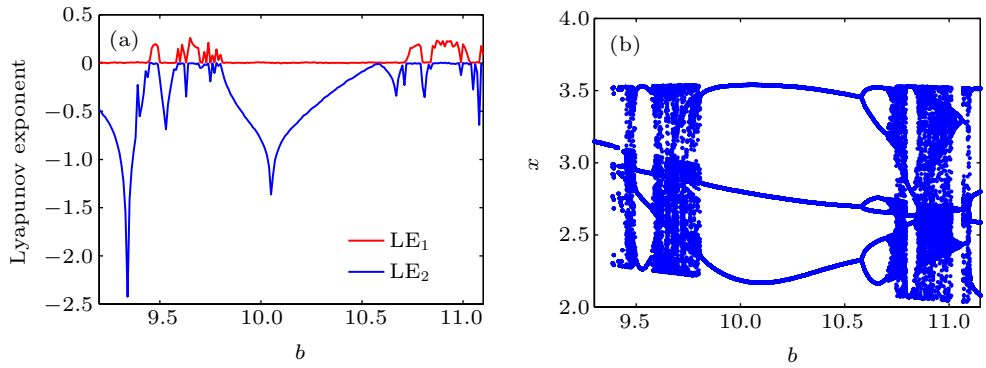


Fig. 20. (a) Lyapunov exponent spectrum and (b) bifurcation diagram changing with parameter b.

Fixing the initial condition $(x_0, y_0, z_0) = (1.298, 0.1, 0.1)$, and changing the circuit parameter b in a range of [9.2, 11.1], the dynamics of the circuit is described by the Lyapunov exponent spectrum and the bifurcation diagram as shown in Fig. 20.

It is seen from Fig. 20 that the system undergoes multi periodic windows and many chaotic regions in a region of $b \in [9.2, 11.1]$, in which there is a period-3 doubling bifurcation process showing complex dynamics.

10. Conclusion and perspectives

In this paper we present a new locally-active memristor. Basic characteristics of the memristor are verified via the POP and the DC V–I plot. We have found that the memristor has two asymptotically stable equilibrium points, $x(Q_0) = 1.298$ and $x(Q_2) = 11.844$ (corresponding to two non-volatile memductances $W(x(Q_0)) = 1.685$ S and $W(x(Q_2)) = 140.280$ S), and exhibits a locally-active region of $-10\ \text{V} < V < -3.095\ \text{V}$. We build a small-signal equivalent circuit at an operating point of the locally-active region to describe the characteristics near the operating point. We prove that the memristor contains an edge of chaos in a voltage interval of $-10\ \text{V} < V < -3.095\ \text{V}$. And we also prove that if the memristor is on the edge of chaos, we can obtain a periodic oscillation by adding an inductor, and we find a chaotic oscillator by considering the parasitic capacitor of the memristor in the periodic circuit, verifying that a locally-active memristor-based system can generate complex behaviors and enriching the connotation of dynamics.

The proposed locally-active model in this paper, when operating in the locally-active region, can generate not only periodic oscillation, but also complex chaotic oscillation, which proves that the simple locally-active memristor model can generate complex behaviors, and that the local activity is bring about all complexities. Therefore, the proposed model can be used in binary memory as a bi-stable device, chaotic oscillator as a locally-active device, chaotic neural network both as an essential device of chaotic oscillation module and as synapse of the neural network.

The proposed memristor can serve as a model to study memristive memory and memristive synaptic plasticity for memcomputing, which can store and process information on the same physical platform. Furthermore, the proposed memristor based chaotic oscillator can be incorporated into a memristive neural circuit for optimizing neural computations in a memcomputing scheme. It will be a challenging task for us to study the locally-active memristor based neural networks with chaotic modules. How to implement memristor-based memcomputing is also one of our future researches.

References

[1] Chua L 1971 *IEEE Trans. Circuit Theory* **18** 507
[2] Chua L and Kang S M 1976 *Proc. IEEE* **64** 209
[3] Strukov D B, Snider G S, Stewart D R and Stanley Williams R 2008 *Nature* **453** 80
[4] Yuan F, Wang G Y and Wang X 2016 *Chaos* **26** 073107
[5] Wang G Y, He J L, Yuan F and Peng C J 2013 *Chin. Phys. Lett.* **30** 468
[6] Sah M P, Kim and Chua L 2014 *IEEE Circuits and Systems Magazine* **14** 12
[7] Xie L and Haron M A B 2016 *IEEE/ACM International Symposium on Nanoscale Architectures (NANOARCH)*, July 18–20, 2016, Beijing, China, p. 85
[8] Prezioso M, Merrikh-Bayat F, Hoskins B D, Adam G C, Likharev K K and Strukov D B 2015 *Nature* **521** 61
[9] Chuang H, Li Y X and Chen G R 2020 *Chaos* **30** 043110
[10] Chen L J, Zhou Y, Yang F Y, Zhong S Z and Zhang J W 2019 *Nonlinear Dyn.* **98** 517
[11] Yuan F, Deng Y, Li Y X and Wang G Y 2019 *Nonlinear Dyn.* **96** 389
[12] Li C L, Li Z Y, Feng W, Tong Y N, Du J R and Wei D Q 2019 *Int. J. Electron. Commun.* **110** 152861
[13] Chua L 2005 *Int. J. Bifur. Chaos* **15** 3435
[14] Mainzer K and Chua L 2013 *The local activity principle: The cause of complexity and symmetric breaking* (London: Imperial College) pp. 146–159
[15] Mannan Z I, Choi H and Kim H 2016 *Int. J. Bifur. Chaos* **26** 1630009
[16] Muthuswamy B and Chua L 2010 *Int. J. Bifur. Chaos* **20** 1567
[17] Chua L 2015 *Radio Engineering* **24** 319
[18] Mannan Z I, Choi H, Rajamani V, Kim H and Chua L 2017 *Int. J. Bifur. Chaos* **27** 1730011
[19] Jin P P, Wang G Y, Lu H H C and Tyrone F 2017 *IEEE Trans. Circuits & Systems II Express Briefs* **65** 246
[20] Ying J J, Wang G Y, Dong Y J and Yu S M 2019 *Int. J. Bifur. Chaos* **29** 1930030
[21] Mannan Z I, Yang C J and Kim H 2018 *IEEE Circuits and Systems Magazine* **18** 14
[22] Mannan Z I, Yang C J, Adhikari S P and Kim H 2018 *Complexity* **2018** 8405978
[23] Weiher M, Herzig M, Tetzlaff R, Ascoli A, Mikolajick T and Slesazeck S 2019 *IEEE Transactions on Circuits and Systems I: Regular Papers* **66** 2627
[24] Chua L 2011 *Appl. Phys. A* **102** 765
[25] Chua L 2014 *Semi. Sci. Tech.* **29** 104001
[26] Chua L 2018 *Appl. Phys. A* **124** 563
[27] Chua L, Sbitnev V and Kim H 2012 *Int. J. Bifur. Chaos* **22** 1230011
[28] Chua L, Desoer C A and Kuh E S 1987 *Linear and Nonlinear Circuits* (New York: McGraw-Hill)
[29] Chua L, Sbitnev V and Kim H 2012 *Int. J. Bifur. Chaos* **22** 1250098
[30] Dogaru R and Chua L 1998 *Int. J. Bifur. Chaos* **8** 211
[31] Sah M P, Mannan Z I, Kim H and Chua L 2015 *Int. J. Bifur. Chaos* **25** 1530010